Nonisothermal Spreading Dynamics of Self-Rewetting Droplets

Non-Isothermal Spreading Dynamics of Self-Rewetting Droplets

Dimitrios Mamalis,[*][†] Vasileios Koutsos,[†] Khellil Sefiane[†]

[†]School of Engineering, Institute for Materials and Processes, The University of Edinburgh, King's Buildings, Edinburgh EH9 3FB, United Kingdom

*To whom correspondence should be addressed: E-mail: d.mamalis@ed.ac.uk

ABSTRACT

We experimentally studied the spreading dynamics of binary alcohol mixtures (and pure liquids for reference) deposited on a heated substrate in a partially wetting situation, under non-isothermal conditions. We show that the spreading mechanism of an evaporating droplet exhibits a power law growth with early-stage exponents that depend strongly and non-monotonically on substrate temperature. Moreover, we investigated the temporal and spatial thermal dynamics in the droplet using infrared thermography revealing the existence of unique thermal patterns due to thermal and/or solutal instabilities which lead to surface tension gradients, namely Marangoni effect. Our key findings are that the temperature of the substrate drastically affects the early-stage inertial-capillary spreading regime owing to the non-monotonic surface tension/temperature dependence of the self-rewetting liquids. At later stages of wetting, the spreading dynamics enters the viscous-capillary dominated regime with the characteristic low kinetics mirroring the behaviour of pure liquids.

INTRODUCTION

Spreading and evaporation behaviour when a droplet impinges on a solid substrate are phenomena encountered in a wide number of physical processes and are of relevance to many technological fields such as microfluidics, coating, ink-jet printing technologies, material processing [1–8]. Indeed, droplet wetting, spreading and evaporation are of key importance for many applications and the underlying mechanisms of these phenomena are still under investigation and are recognised as crucial in a wide range of biological, natural and industrial processes [9–12]. The spreading and evaporation of a liquid over a solid surface is a complicated free-boundary problem characterized by the presence of a moving contact line involving three phase (liquid, vapour, and solid) interactions through coupling by conduction with the substrate, convection/conduction within the liquid drop and convection/diffusion in the vapour phase. When the fluid impacts on a solid surface, it is initially in a transient, capillary flow and the wetted contact area moves until the liquid-solid-vapour system reaches an equilibrium state with a minimum energy configuration. The first moments of spreading behaviour tend to be rapid and the nature of the boundaries governing the dynamics on how the drop reaches a stationary state vary depending on parameters such as surface chemistry, liquid physicochemical properties and environmental conditions [1,3,6,13].

Many experimental and theoretical studies have been devoted to understanding the evolution of the internal flows generated within a spreading and evaporating liquid droplet, and have a drastic effect on the wetting kinetics. These generated flows within the droplets are significantly affected by liquid viscosity, surface tension forces, density and the wettability of the substrate surface, hence influencing the spreading behaviour of the liquid. However, applying heat (by e.g. a heated substrate) to a liquid phase, the

evaporation rate is increased inducing high temperature imbalances within the drop and in turn generating variations of the physical properties. Temperature variation at the interface induces non-uniform thermal energy exchanges influencing significantly the evaporation mechanism and in turn affecting the wetting state. These interactions between wetting transitions and surfaces have been one of the most active sub-disciplines in the field of liquid phase transitions over the last two decades [14–16].

In the case of single-component droplets, the characteristic flow within the droplet is found to be an outward flow raised from mass conservation to replenish fluid evaporating preferentially at the outer edge of the droplet [9,17,18]. During the evaporation of volatile droplets, thermocapillary instabilities, known as Marangoni instabilities, are developed when the system is subjected to sufficiently strong surface tension gradients. The origin of this fluid flow, in volatile liquid droplets, is the Marangoni flow which is driven by surface tension instabilities along the surface of the liquid due to temperature gradients [10,18]. Bénard [19] and later Pearson [20] presented a theoretical investigation about the role of surface tension in this phenomenon. Ghasemi *et al*. reported that the flow in an evaporating water droplet which is in a reduced pressure environment is driven mainly by thermocapillary convection *i.e.* temperature gradients [21]. This pointed out the important role of the Marangoni flow in the energy transport mechanism, as the evaporation rate increased in the case of reduced pressure conditions. The significant contribution of Marangoni stresses, i.e. intensity and orientation of the generated flows, in a single-component system depends on the relative thermal properties of the substrate and the liquid, the experimental conditions and liquid geometry [22–25]. Generally, surface-tension-driven flows in single-component volatile droplets, e.g. water, are essentially thermocapillary in nature.

For binary and generally multicomponent droplets the physical behaviour poses many challenges as it can be more complex. Previous studies with droplets formed from binary mixtures of water with alcohol (methanol [26], ethanol [27–30] and 1-propanol [31]) showed a rather complicated behaviour during the evaporation process compared to those of pure liquids. The evaporation mechanism of these binary mixtures in particular involves three distinct stages; a first stage, where the more volatile component (alcohol) migrates to the liquid interface and in principal evaporates first, a second stage which is transitional and involves evaporation from both components (mixed stage) and a last stage which mainly consists of the evaporation of the less volatile component of the mixture although residual amounts of the alcohol phase may still exist in the solution [26–28,32,33]. Moreover, it is thought that the final stage of evaporation mirrors the behaviour of pure liquids.

Previous studies investigating the first seconds of an spreading droplet evaporating on a solid surface revealed that the underlying causes of the observed mechanism are related to inertia, capillary and viscous forces [1,3,6,34]. More specifically, during spreading, the contact line moves radially outwards from the contact point and the droplet wets a circular area of radius $r(t)$. The unbalanced horizontal Young force: $\gamma(\cos\theta - \cos\theta_{eq})$ drives the droplet to spread on the substrate until it reaches the final equilibrium contact angle θ_{eq}, where γ is the liquid-vapour interface surface tension and θ the instantaneous contact angle. Numerous experimental and theoretical studies of spreading droplets have shown that an inertial regime exists ahead of the viscous regime [35–41]. This rapid early stage of wetting lasts only a few milliseconds and, for completely wetting surfaces, it is well described by an exponential power law, $r \sim t^{1/2}$.

4

Here, the characteristic inertia time scale τ_ρ for the early stage of spreading is $\tau_\rho \sim \sqrt{\rho R^3/\gamma}$, where R is the initial droplet radius before contact and ρ is the liquid density [37–40,42]. Bird $et\ al.$ found that the short-time spreading dynamics depends strongly on surface wettability due to capillary wave generation, leading to a non-universal exponent that varies with the equilibrium contact angle θ_{eq} [38]. The authors demonstrated that the initial contact line dynamics was affected by the surface chemistry and the volume of the liquid droplet, whereas the fluid viscosity was not a crucial factor. Interestingly, more recent investigations for droplets spreading on partially wetting surfaces revealed that the early times dynamics (immediately after initial contact) are independent of the surface wettability, with an exponent ~0.5 (best fit exponent: 0.48) consistent with the inertia $\left[\sim \rho\left(dr/dt\right)^2\right]$ and the capillary ($\sim \gamma \cdot R/r^2$) pressure balance [40]. Additionally, in the final stage of spreading, it is well known that the spreading dynamics is governed by the Tanner's law which emerges by balancing capillary and viscous forces and relates the radius of the wetted area with time as $r \sim t^{1/10}$ [6,39,43]. The spreading dynamics in this regime is characteristically slow; if the capillary forces driving the flow are primarily hindered by viscosity, the natural timescale is $\tau_\mu \sim \rho R/\gamma$.

Vochten and Petre were the first to report that for dilute aqueous solutions of high carbon alcohols (number of carbon atoms $\geq$ 4), the temperature dependence of the surface tension showed a minimum at certain temperatures and the surface tension dependence turned to be positive in the higher temperature region beyond the bounds of the minimum [44]. This behaviour leads to a non-linear thermocapillary effect which was studied by Oron $et\ al.$ [45] and later by Slavtchev and Miladinova [46]. Dilute aqueous

solutions of alcohols such as butanol, pentanol, hexanol etc. can be considered ''self-rewetting'' fluids because of the anomalous (non-monotonic) dependency of the surface tension with temperature in a range of concentration [47–50]. These solutions experience a well-defined minimum in surface tension dependence on the temperature i.e. (quasi-parabolic) non-linear behaviour, where the surface tension increases as the temperature rises above a certain point. Thus, for evaporation based applications (such as heat pipes) in which the temperature will rise as the outbreak of dry-out occurs, these alcohol mixtures ''self-rewet'' by moving towards the hot spots where the surface tension is increased and enhance the heat transport rate and the thermal performance of the systems [51]. These binary fluids have recently been investigated by many researchers and are proposed as new innovative operating fluids for advanced heat transfer technologies, e.g. heat pipes or heat spreaders for terrestrial and space applications [51–58]. Figure 1 gives an illustrative plot of the behaviour of ordinary liquids and self-rewetting aqueous alcohol solutions as a function of temperature. Since these solutions contain a water fraction in excess of the azeotropic composition, the alcohol-rich component preferentially migrates in the course of liquid/vapour phase change and evaporates first. In turn, this results in concentration gradients in the liquid/vapour interface. The presence of liquid–vapour gradients (concentration and/or temperature) at the vicinity of the triple contact line leads to spontaneous liquid inflows directed from the colder region to the hotter side, for temperatures above the minimum of the surface tension (Figure 1). In this case, the convection mechanism is driven by the reverse Marangoni effect [59,60]. Therefore, the induced Marangoni convection flows may play an important role in energy transport phenomena [21,61,62].
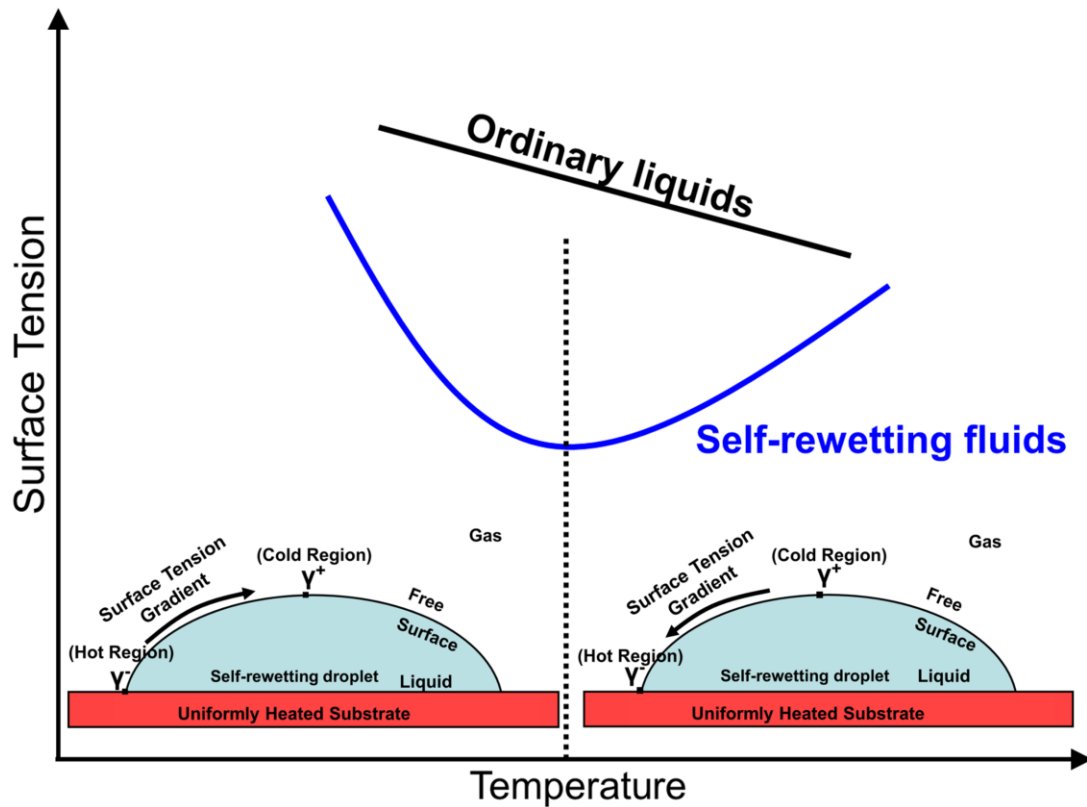
Figure 1. Ordinary liquids (black line) and binary alcohol mixtures (blue line) surface tension dependence with temperature and schematic view of the Marangoni effect for self-rewetting droplets on a heated substrate as surface tension gradients are induced at the liquid/vapour interface.

Multiphase flows coupled with heat transfer mechanisms still pose many experimental and theoretical challenges. In this work, we study for the first time the spreading dynamics of self-rewetting droplets which partially ($90^\circ > \theta_{eq} > 0^\circ$) wet a flat uniformly heated substrate under non isothermal conditions. We particularly focused on the first seconds of the wetting behaviour for two cases of alcohol mixtures: water – 1-butanol 5% vol. and water – 1-pentanol 2% vol. We also experimentally investigated for the first time, using IR thermography, the flow patterns in the spreading evaporating droplet arising from the contact with different heated substrates and the non-uniform evaporation which drastically affect the wetting ability and thus the spreading

mechanism. The nature and the evolution of the complex thermal patterns (internal flows) generated within the spreading binary droplets were discussed in terms of contact line dynamics, heat transfer phenomena and the contribution of Marangoni convection.

EXPERIMENTAL METHOD

The first step in our experiments was to prepare solutions using pure alcohols: 1-butanol (Sigma-Aldrich Co. LLC. 360465) and 1-pentanol (Sigma-Aldrich Co. LLC. 398268) with specific concentrations: water – 1-butanol 5% vol. and water – 1-pentanol 2% vol. For each measurement a binary droplet with constant concentration, temperature and with a volume in the range from 1 μL to 5 μL was placed onto an ethanol-cleaned borosilicate glass microscope coverslip (dimensions: 24 mm × 50 mm × 100 μm purchased from TAAB Laboratories Equipment Ltd, U.K.). Borosilicate glass is a type of glass with silica and boron trioxide as the main glass-forming components and it is characterised by varying hydrophilic nature depending on the chemical composition of the used glass family. It has a very low thermal expansion; $3.3 \times 10{-6}$ K^{-1} at 20°C – 300°C, and low thermal conductivity; 1.14 W/mK at 20°C and 1.2 W/mK at 90°C. Moreover, a corrosion-resistant ceramic (AlN) substrate (Valley Design Corp.$^{®}$) was used to perform experiments regarding self-rewetting droplets. The aluminium nitride substrate (25.4 mm sq. × 127 μm thk.) is characterised by a low thermal expansion (4.5 × 10^{-6} K^{-1} up to 700°C) and relatively high thermal conductivity for an electrically insulating ceramic, around 175 W/mK (polycrystalline material). A surface roughness tester, SURFTEST SJ-410 series (Mitutoyo Corporation, Japan), was used to measure the height surface profiles of the substrates. Then, the roughness values Ra (average) of the samples were calculated. Ra is the arithmetic average value of the departure of

the profile above and below the mean line throughout the specified sampling length. The surface sampling length selected in this evaluation was 15 mm while the scan speed was 0.1 mm/s. The surface roughnesses of the borosilicate glass and AlN substrates were 0.21 μm and 0.26 μm, respectively. A flexible silicone rubber heater SRGF-203/5-P-230V (Silicone Rubber Fiberglass Insulated Heaters), provided from OMEGALUX®, was placed underneath the glass coverslip and the ceramic (AlN) substrates for uniform heating. The heater was connected to a dedicated proportional–integral–derivative (PID) controller purchased from Cole-Parmer®. A digital camera and a diffuse light source was placed on either side of the recording droplet during the whole spreading process. The substrates were placed horizontally and care was taken to reduce the convective air currents around the droplet due to the light source. The syringe pump was set at a constant volume rate of 1 μL/min and a pendant droplet was grown at the needle tip, until it touched the heated substrate. Digital images of the sessile spreading droplets were recorded at 0.0167-second intervals and analysed using the FTÅ200, Dynamic Contact Angle Analyzer software (First Ten Ångstroms, Inc., Portsmouth). At early times of spreading when the droplet was a spherical cap the profile was fitted using Young-Laplace equation [63] and values for the droplet base radius r, height h, volume V, surface area A and contact angle θ were extracted from the dedicated software. Pendant drop method analysis was used to measure interfacial tension of the fluids using the FTÅ200 apparatus. This method involves the determination of the profile of a drop of one liquid suspended in another liquid or fluid at mechanical equilibrium. The profile of these drops was determined by the balance between gravity effect and the surface forces. More specifically, a heating bath regulator containing water (and placed next to the FTA apparatus) was used to set the required temperature of the liquids. Syringes (2mL) with the desirable liquids were dipped in the heated bath

until reached the set temperature. Thermocouples (K-type) were placed in the heated water bath and in the core of the syringe to control accurately the temperature of the liquids, concurrently. The front side (tip) of the syringe was sealed before immersion in the heated bath, using a high temperature (up to 300ºC) tacky (but easy to remove) tape with excellent resistance to water, water vapour, and alcohols. Since the time that was needed to remove the syringe from the bath place it in the pump driven motor system of the FTA apparatus, and subsequently extract a pendant drop resulted in a small temperature decrease of the liquid, the bath was set at a slightly higher temperature. In this way, we accounted for the inevitable small drop during the transfer. Furthermore, the use of thermocouples in the core of the syringe helped to monitor the temperature and reach the desire temperature for our experimental study with an error of ±1ºC. The surface tension measurements were repeated several times (around 15 repetitions), for each temperature and for each liquid case examined. In addition to the drop shape analysis goniometer (FTÅ200) measurements, a ThermaCam^{TM} infrared thermography camera (SC3000 Series, FLIR Infrared Systems, 2005) was also used to analyse the surface temperature profiles of droplets of the same range size and concentration. The ThermaCam^{TM} SC3000 offers ultra-high thermal sensitivity, broad dynamic range and revolutionary long-wave imaging. The GaAs, Quantum Well Infrared Photon FPA detector of the camera has spectral range between 8 and 9 μm in the longwave infrared spectrum with a high resolution of 320 x 240 pixels, thermal sensitivity of 20 mK at 30°C and an accuracy of ±1°C for temperatures up to 150°C. The infrared camera detector is Stirling cooled to 70 K with cool down time < 6 min. The images were obtained at 50 frames/s using a camera fitted with a microscope lens with 10×7.5 mm^2 field of view and 26 mm minimum focal length. The infrared system provides automatic transmission correction of temperature, based on atmospheric

temperature, relative humidity, input distance from the object and emissivity of the object. The IR camera was used with a dedicated PC for acquisition, with specialized software (ThermaCAM Researcher Professional 2.9®) for image post-processing. The emissivity of the binary mixtures was close to that of pure water (~0.95) and it is a fixed parameter to accurately measure the liquid surface temperatures [14]. It is worthwhile noting that the emissivity of the pure 1-butanol droplets was dependent on the liquid thickness [14], as it is a semi-transparent fluid to IR at the camera wavelengths of $8 - 9$ μm. Thus, in our present study, the obtained IR measurements for the butanol cases must be interpreted with care as the IR camera gave an indication of the temperature profile of the liquid close to the liquid interface but not of the interface itself [13]. The total energy measured from the IR camera was the emission of the energy coming from the solid (glass substrate), the reflection of ambient radiation from the liquid-vapour and liquid-solid surfaces, and the emission from the bulk of the liquid (due to its small liquid thickness). For this part of the experiment, the droplets were deposited onto the glass coverslip and the ceramic substrate by means of a syringe pumping device. The substrates were heated-up uniformly in the same way as with the experiments conducted with the FTÅ200 apparatus. The thermal imaging camera was vertically mounted at the top of the droplet. Before performing the experiment, we checked that substrate temperature homogeneity was stable at $\pm 0.5°C$ with the use of thermocouples (K-type) in addition to the adopted PID controller. The infrared camera recorded radiation coming from the fluid volume and the heated substrate and the spatial and temporal temperature data of the droplet surface field were acquired. Figure 2 illustrates the experimental setup for the dynamic and thermal measurements of the droplets. It has to be noted that experiments performed by using the two cameras both simultaneously and individually. Both pure liquids and binary alcohol mixtures

11

temperatures were kept constant at 9º±1º C using a heating-cooling bath regulator before performing the experiments. The air temperature and the relative humidity surrounding the slide glass were $T = 18\pm1ºC$ and $RH = 45 \pm 5\%$, respectively, and the atmospheric pressure was assumed to be at $P = 1$ atm.
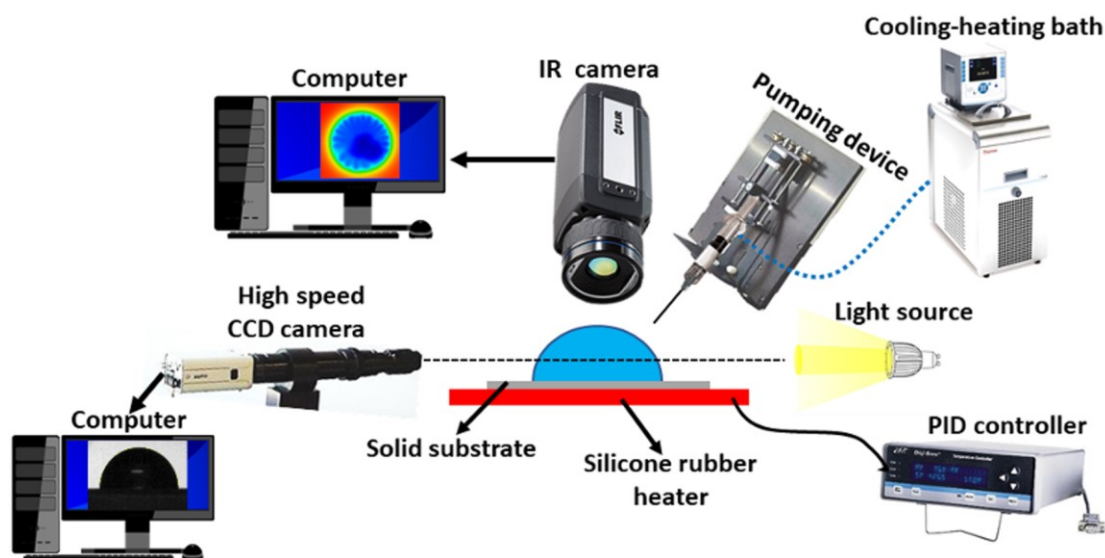

Figure 2. Schematic illustration of the experimental apparatus.

RESULTS

The first step in our experiments was to compare the spreading behaviour of the pure liquids: (a) pure water and (b) pure butanol, with those of the dilute aqueous solutions of high carbon number alcohols: (c) water − 1-butanol 5% vol. and (d) water − 1-pentanol 2% vol., under controlled experimental conditions. Figure 3 presents the sessile droplet contact base radius r adjustments, i.e. the difference between the final r_{max} (at equilibrium contact angle, θ_{eq}) and initial value r_0 (immediately after deposition), for three different temperatures: 30ºC, 60ºC and 90ºC, in a volume range from 1 to 5.5 ±0.2 µL, onto the uniformly heated glass substrate. Note that the obtained values represent typical examples i.e. among six or more repetitions for each droplet

volume and for each temperature, of all measurements were carried out. Pure liquids base radius change followed a linear increase with temperature, Figure 3 (a) and (b), contrary to the alcohol mixtures where the non-monotonic dependence of the wetted contact radius with the temperature was revealed, Figure 3 (c) and (d).
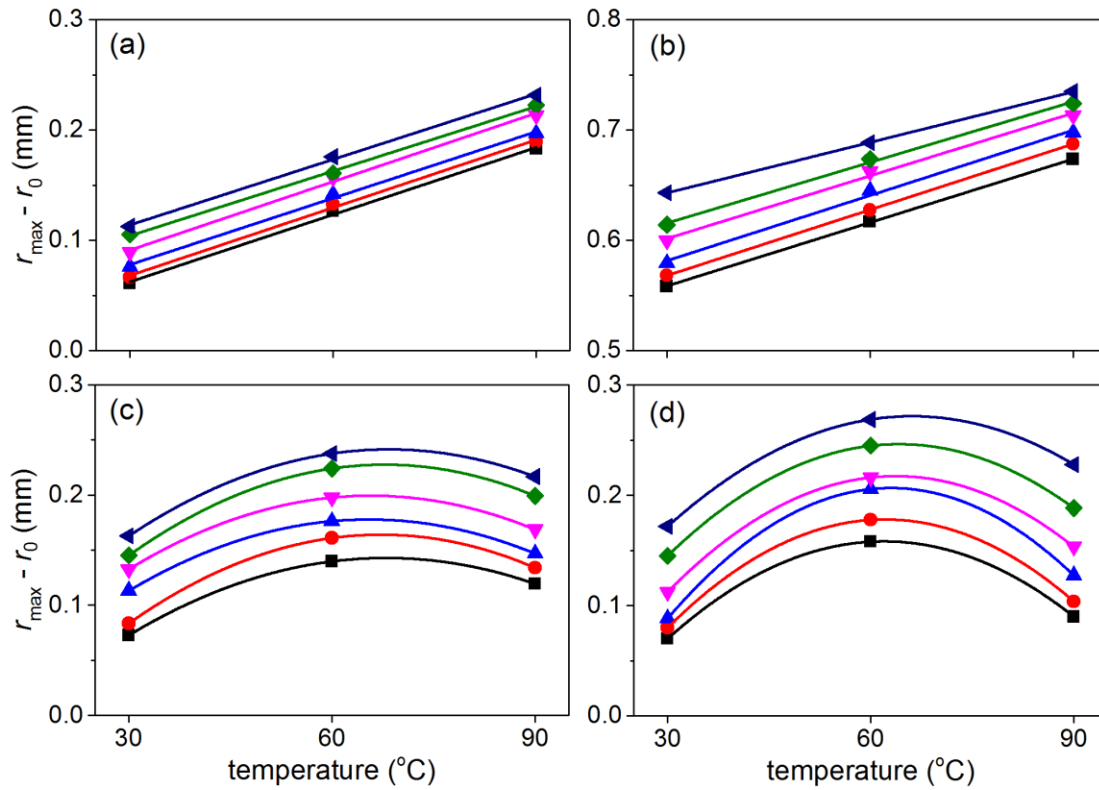

Figure 3. Droplet contact radius changes (difference between the final, r_{max}, and initial, r_o, contact base radius) for pure liquids: (a) pure water, (b) pure butanol, and binary mixtures: (c) water – 1-butanol 5% vol. and (d) water – 1-pentanol 2% vol., with volumes: 1(■), 2(●), 3(▲), 4(▼), 5(◆) and 5.5(◄) ±0.2 µL, against the three different temperatures: ~30ºC, ~60ºC and ~90ºC, on a uniformly heated glass substrate, under ambient conditions.

The surface tension of the ordinary liquids (pure water and pure 1-butanol) and the self-rewetting fluids (binary alcohol mixtures) has been measured in the temperature range from ~10ºC to ~90ºC, using the pendant drop method analysis (FTÅ apparatus). Typical

results are shown in Figure 4 where it is clearly depicted the linear decrease of the surface tension of the pure liquids with increasing temperature (Figure 4 (a)). Note that the pure 1-pentanol case was not plotted due to the relatively similar surface tension values with the pure 1-butanol case in this temperature range $(10 - 90 \pm 1 \, ^{o}C)$. Moreover, the non-linear (quasi-parabolic) and non-monotonic dependence of the surface tension of the self-rewetting droplets with the temperature can be seen in Figure 4 (b). The minimum of the surface tension was measured around $63 \, ^{o}C$ and the unusual temperature dependence which turns out to be increasing in the higher temperature region beyond the minimum for these self-rewetting solutions was clearly revealed. The surface tension measurements showed good agreement with previous work that have been reported from previous experimental studies using these (self-rewetting) binary alcohol mixtures [51,53,54]. It is worth noting that the results presented in Figure 3, can be interpreted based on the measurements of surface tension, Figure 4. It can be observed that the increasing wettability of the pure liquid droplets was attributed to the surface tension dependence on temperature. Additionally, the non-monotonic dependence of the surface tension with the temperature for the binary alcohol droplets was revealed on the overall spreading behaviour where beyond the minimum of the surface tension (at $\sim 63 \, ^{o}C$) the wettability of the droplets was decreased. To minimise further the uncertainties of the measurements of the surface tension values of the examined liquid cases in this temperature range, several repetitions (around 15 repetitions for each temperature and each liquid) were performed.
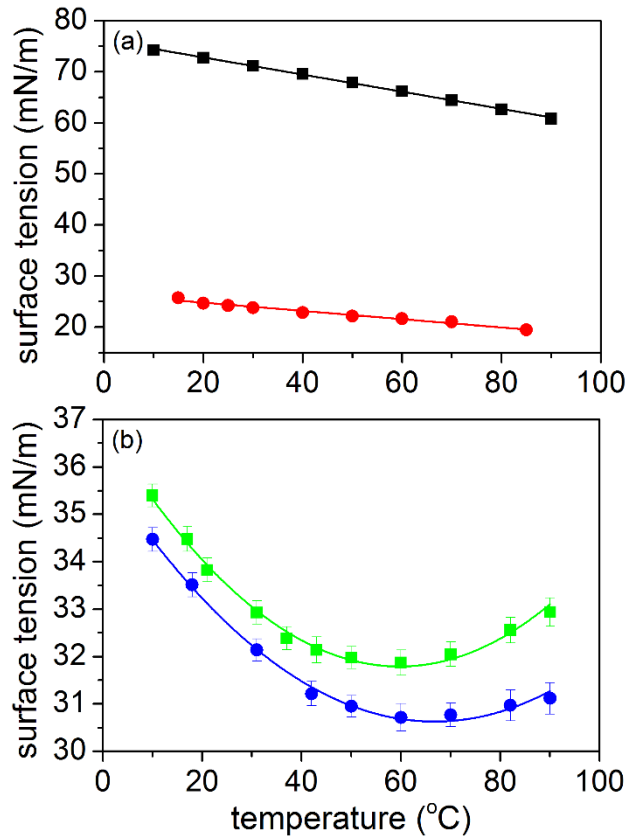
Figure 4. Surface tension measurements (mN/m) of the (a) pure liquids: pure water (■) and pure 1-butanol (●) and for the (b) self-rewetting fluids: water – 1-butanol 5% vol. (●) and water – 1-pentanol 2% vol. (■), in the temperature range from around 10ºC to 90ºC, under controlled experimental conditions. Note that the curves represent average values with obtained errors (among fifteen or more repetitions for each temperature) of all measurements performed.

The spreading contact base radius $r(t)$ of the binary mixtures sessile droplets at the early stage (tenths of second) of spreading for a range volume from ~1 to ~5 µL, was systematically measured. Typical results of the binary droplets with volumes: 2±0.2 µL and 4±0.2 µL, for three different temperatures ~30, ~60 and ~90 ºC (of the heated substrate) are presented in Figure 5, respectively. The results showed how the wetted radius r of the binary alcohol mixtures developed over time t once a droplet contacted onto the uniformly heated substrate; this early stage regime is usually dominated by inertia-viscous contributions. Since in the study we focus on the first-early stage of drop

15

spreading rather than on the overall drop lifetime, the complete drop evaporative behaviour is not included in Figure 5. The results demonstrated that for each temperature of the substrate, binary droplets spread at a different speed rate. In particular, for ~90°C, alcohol droplets showed increased kinetics, hence reaching a maximum radius much quicker than that of other cases. At around 60°C, the binary droplets was seen to spread much more in comparison with the other substrate temperatures which is consistent with the surface tension minimum (about 63±1°C), as shown in Figure 4. It is clear that at ~60°C substrate temperature, the surface tension forces dominated and resulted in the enhancement of the spreading dynamics, as reported in previous studies [35,36,38,40]. The overall surface tension of the water-butanol mixture was slightly lower than that of the water-pentanol mixture (see also Figure 4) due to the different alcohol concentrations (5% vol. and 2% vol.) used for these binary alcohol mixtures. In turn, this can affect the overall wetting of the self-rewetting droplets. It is clear that the depletion time of the alcohol phase in these two self-rewetting droplets was different (quicker for the water-pentanol mixture) at the same substrate temperatures.
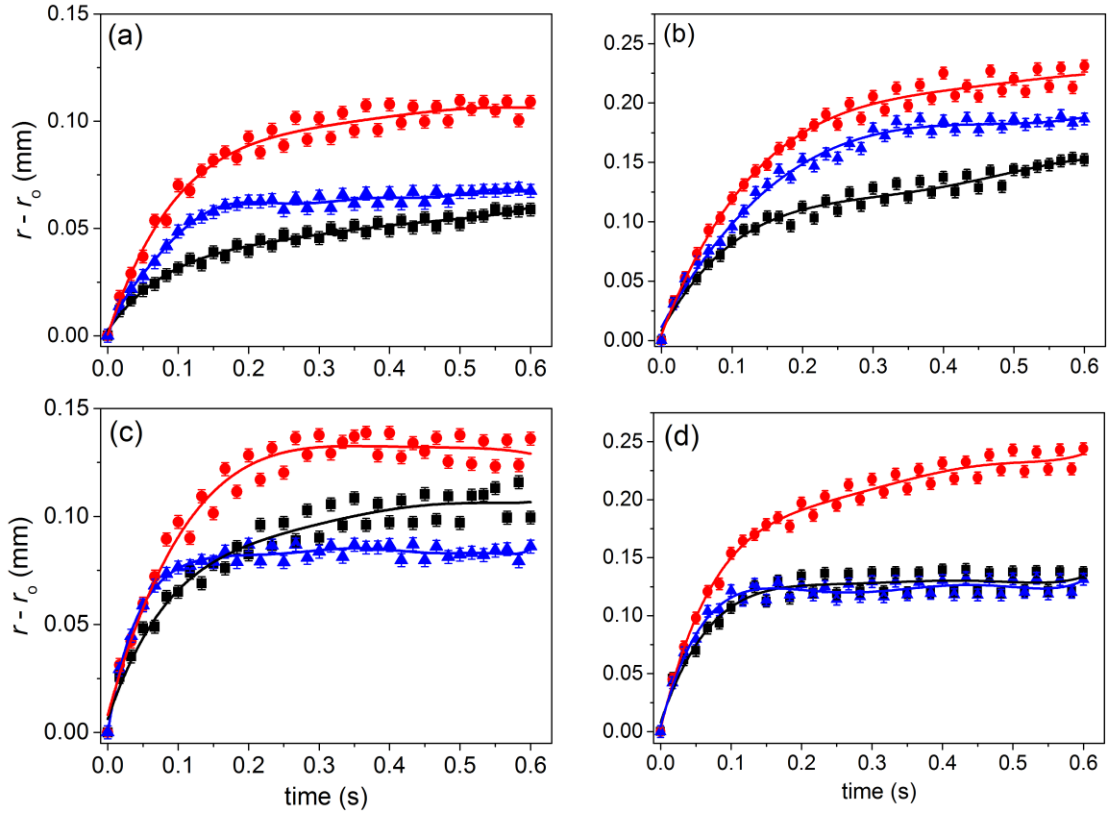
Figure 5. Evolution of the contact radius r (mm) of the wetted area for water – 1-butanol 5%

vol. droplets: (a) 2±0.2 μL, (b) 4±0.2 μL and for water – 1-pentanol 2% vol. (c) 2±0.2 μL and

(d) 4±0.2 μL as a function of time t (s), for three different temperatures: ~30°C (■), ~60°C (●)

and ~90°C (▲), respectively. Note that the obtained curves represent typical examples (among

six or more repetitions for each droplet volume and for each temperature) of all measurements

performed. Uncertainties observed in wetted radius r measurements are due to the FTÅ

apparatus errors, around 3%.

Following the above observations about the spreading behaviour of the self-rewetting

droplets on glass slides and the underlying spreading kinetics, an in-depth analysis

focusing on the profile of each stage of spreading was conducted. Typical log-log plots

of the spreading dynamics, for both self-rewetting mixtures examined and for four

temperatures (20, 30, 60 and 90 ±1 °C), are presented in Figure 6 (a) and (c). For the

calculations of the contact radii, the shape of the sessile drops were approximated by a

parabolic function. This is a good approximation that has been used extensively in the literature, even in the presence of Marangoni flows [64]. It can be clearly seen that spreading occurs in two characteristic stages i.e. inertia and viscous spreading regimes, and a transition regime in-between [35–40,42]. The unbalanced horizontal force: $\gamma_T(\cos\theta - \cos\theta_{eq})$ drives the droplet to spread on the heated substrate until it reaches the final equilibrium contact angle θ_{eq}, where γ_T is the liquid-vapour interface surface tension (at specific temperature T) and θ the instantaneous contact angle [35–38,40,42]. It was found that once the liquid droplet has established contact with the surface, the extension of the contact line radius $r(t)$ follows an exponential power-law ($r - r_0 \sim t^n$) of rapid growth, for all the experiments performed. In both graphs (a) and (c) (Figure 6), the power law (growth) has an exponent n which depends strongly on the substrate temperature T. Additionally, experimental results related to the evolution of the contact angle in time are presented in Figure 6 (b) and (d) for the respective cases of water – 1-butanol 5% vol. and water – 1-pentanol spreading droplets as seen in Figure (a) and (b). A sharp decrease of the contact angles were noticed in the initial wetting stage connected with the different substrate temperatures. It can be clearly seen that the binary droplets resulted in faster and improved spreading mechanism as the temperature of the substrate was increased, at equivalent times. This (non-linear) decay of the contact angles is in agreement with the (non-linear) growth of contact radius of the self-rewetting spreading droplets.
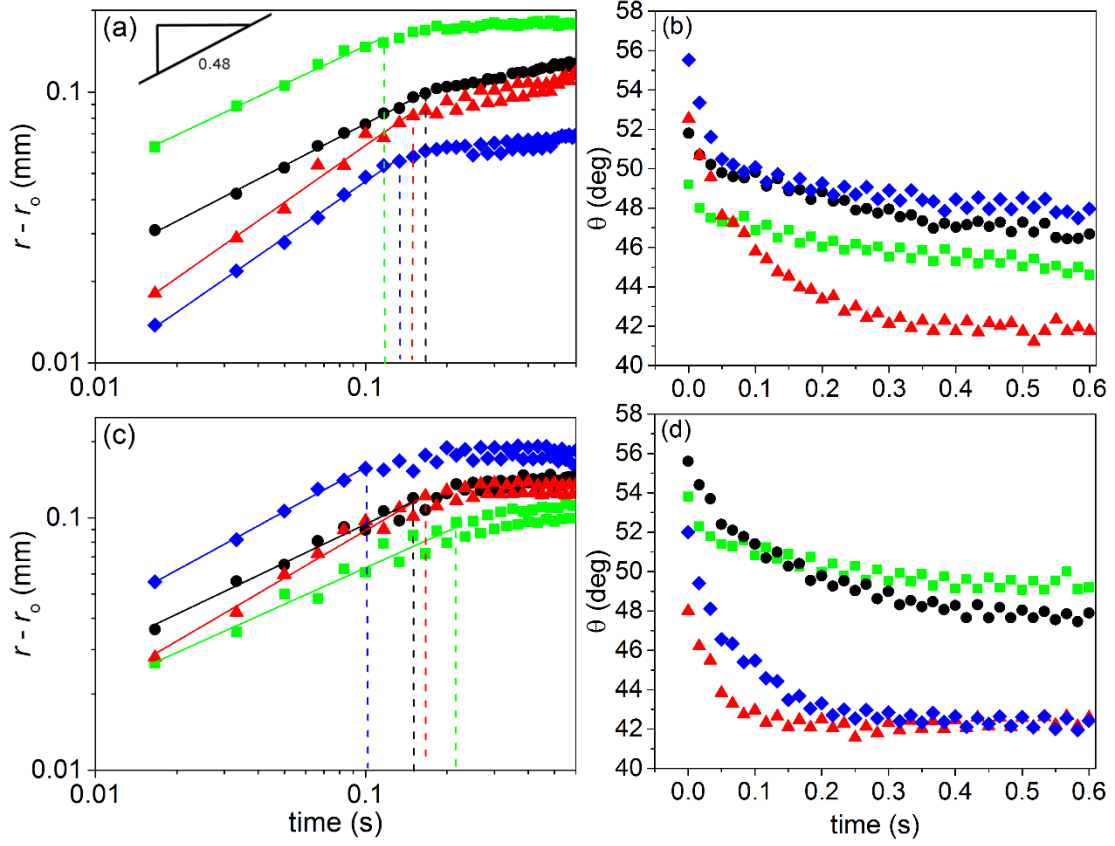
Figure 6. log-log plot measurements of the contact radius r (mm) as a function of time t (s) (volumes $3 - 4 \pm 0.2$ μL) for four different substrate temperature cases: ~20°C ($\blacksquare$), ~30°C ($\bullet$), ~60°C ($\blacktriangle$) and ~90°C ($\blacklozenge$) for the (a) water – 1-butanol 5% vol. and (c) water – 1-pentanol 2% vol. droplet solutions, respectively. The spreading follows a power-law (growth) over time ($r - r_o \sim t^n$) with different exponents n (n_{1st}; first stage which approximately lasts for a period until the dashed lines in each curve). Note that at the later times of spreading (second stage of spreading), slow capillary-viscous dynamics with exponents $0.1 < n_{2nd} < 0.2$ governed the wetting mechanism of the self-rewetting droplets. Evolution of the contact angles θ in time for the (b) water-1-butanol 5% vol. and (d) water – 1-pentanol 2% vol. spreading droplets. Uncertainties observed in wetted radius r and contact angles θ measurements are due to the FTÅ apparatus errors, around 3%.

19

Table 1 presents both the first (inertial-capillary) n_{1st}, and second (capillary-viscous) n_{2nd}, stage exponents, for water-butanol 5% vol. and water-pentanol 2% vol. droplets, respectively, for the data shown in Figure 6. The obtained spreading exponents (Table 1) quantify the spreading droplet kinetics on the heated substrate at the early times of wetting in connection with the thermocapillary-driven flows generated due to surface tension forces gradients at the air-liquid interface. Before we discuss the values of the exponents in the different regimes, it is important to note that the first (inertial-capillary) regime lasts only a few milliseconds (Figure 6) in excellent agreement with the values of the characteristic inertia time scale, $\tau_\rho \sim \sqrt{\rho R^3 / \gamma}$, (where R is the initial droplet radius before contact and ρ is the liquid density) calculated to be in the range of 0.08 to 0.25 s for all the different cases (different volumes, temperatures and liquid properties), in our experiments. Initially, when the substrate temperature changed from ~20°C to ~30°C, a slight increase of the n_{1st} can be observed from ~0.48 to ~0.51 (Table 1) in both binary droplets. As the temperature of the substrate increased from ~30°C to ~60°C, the obtained n_{1st} spreading exponents for water-1-butanol and water-1-pentanol droplets increased to ~0.71 and ~0.61, respectively. At ~90°C of the surface temperature, the 1-butanol aqueous droplet achieved an n_{1st} exponent of around 0.69 while the 1-pentanol mixture obtained a n_{1st} value of 0.52. Furthermore, it is clear that the later times of spreading were characterised by slow wetting dynamics, since the system was dominated by viscous-capillary forces and approximately followed the well-known Tanner's law described as: $r - r_o \sim t^{1/10}$ [43]. The n_{2nd} (second stage) power-law exponents were calculated to be from ~0.1 to ~0.2, in all cases examined. Another important feature revealed was the presence of a transition regime in the spreading profile of the droplets between the first and second stages. The latter corresponded to the shift from inertial to viscous spreading regions which lasted as long

as the capillary wave became pronounced over the bulk of the liquid. Upon droplet deposition on the surface, the capillary wave generated at the bottom of the drop, propagates upwards to the top of the drop and then back while the contact line is moving. However, the generation and propagation of the capillary wave initiated at the contact line may be the rate limiting process as there is a critical wavelength below which surface tension forces dominate the capillary wave propagation [38,41]. Thus, in our cases, the observed transition regime may explain the slightly higher exponents obtained for the second stage of wetting compared to the Tanner's law, in agreement with previous studies [39,40,42].

Table 1. Spreading exponents values for the water-butanol 5% vol. and water-pentanol 2% vol. solutions regarding the two stages of wetting on the glass substrates at the four different (uniform) substrate temperatures: 20, 30, 60 and 90 ±1 °C.

Temperature (°C)	Water – 1-butanol exponent		Water – 1-pentanol exponent	
	$\sim n_{1st}$	$\sim n_{2nd}$	$\sim n_{1st}$	$\sim n_{2nd}$
20	0.48	0.12	0.48	0.13
30	0.51	0.16	0.51	0.11
60	0.71	0.15	0.62	0.12
90	0.69	0.11	0.58	0.11

Figure 7 shows the average (arithmetic mean) values (five or more repetitions for each case of volume and temperature) of the spreading exponents for the pure liquids and the binary mixtures against the three characteristic substrate temperatures, in a volume range from 1 to 5 ±0.2 μL, under controlled non-isothermal conditions on heated glass surfaces. The spreading exponent n for the pure liquids increased weakly (and linearly) with increasing temperature in both of the two characteristic stages of spreading, as can be seen in Figure 7 (a) and (b). The behaviour of the exponents of the pure wetting droplets is consistent with the dependence of the surface tension on the temperature and

21

with the argument that surface tension governs and dominates the short-time wetting dynamics. Binary solutions of alcohols, on the other hand, revealed a non-linear and non-monotonic dependence of the spreading exponent n with increasing temperature in the first spontaneous stage of wetting. It is worth mentioning that the existence of a local maximum in the n_{1st} exponent, for both binary alcohol mixtures, at substrate temperature of ~60°C, is consistent with the surface tension dependence on temperature and the well-defined minimum, as seen in Figure 4. In the second stage of wetting, Figure 7 (d), alcohol mixture droplets were characterized by slow dynamics (viscous-capillary region) with various low spreading exponents $0.1 < n_{2nd} < 0.2$, for each temperature examined. The motion of the sessile self-rewetting droplets on such a non-isothermal state is mainly driven by the (strong) Marangoni stresses due to surface tension gradients induced by temperature and compositional imbalances. Surface tension will continue to drive spreading in the viscous regime until the droplets reaches their equilibrium contact angle θ_{eq}. It has to be noted that in the case of 90°C substrate temperature, initially the surface gradients are directed from hot to cold regions (similar direction as presented at 30°C and 60°C cases). As time evolves and the liquid is heated up from the contact line, the temperature of the liquid will go above 60°C and the surface tension driven flows will change direction towards hot regions from cold regions (for the part of the droplet that is T>60°C); reverse Marangoni effect. However, the overall surface tension gradients during spreading behaviour of the self-rewetting droplet will be directed from hot to cold regions as seen in the previous cases due to the small surface tension differences in the range from 60°C to 90°C (as seen in Figure 4) as well as from the rapid heating of the liquid. Remarkably, the effect of the reverse Marangoni effect was revealed in both mixture cases (more clear in water-pentanol cases) as it is evident by the slight decrease of the spreading exponents from 60°C to

90°C cases causing the spreading contact line to slow down, decreasing the wetting rate due to the redirection of the surface tension driven flows at the periphery of the droplet (at the part of the droplet where T > 60°C).
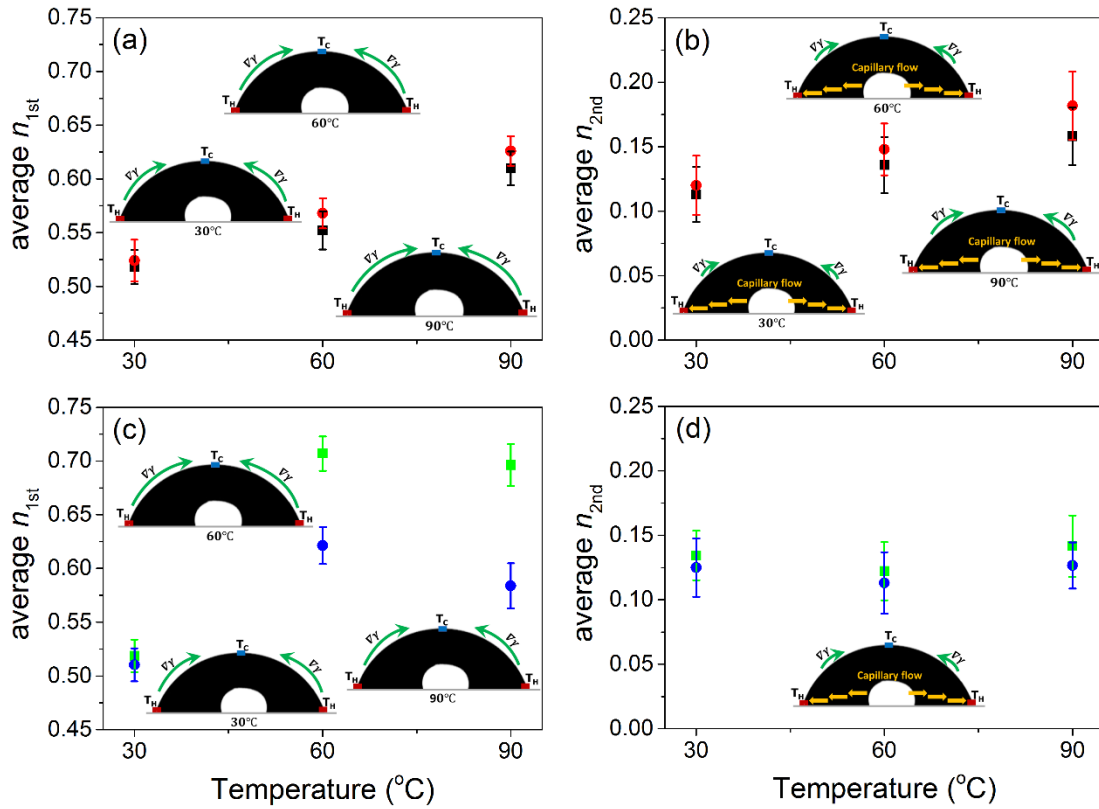

Figure 7. Average values (at least five repetitions for each case of volume and temperature) of the spreading exponents, *n* for the two characteristic stages of wetting versus the three typical substrate temperatures: ~30, ~60 and ~90 °C, for the pure droplets: (a, b) water (■) and butanol (●) and (c, d) binary alcohol droplets: water – 1-butanol 5% vol. (■) and water – 1-pentanol 2% (●), under controlled experimental condition. The error bars obtained among six or more repetitions for each droplet volume and for each temperature of all measurements performed. Note that the droplet insets in each image illustrate the direction (and strength) of the surface tension gradients acting at the liquid-air interface during wetting as well as the capillary flow at later times of spreading (n_{2nd}).

To gain a further understanding of the droplet short-time spreading behaviour under various substrate temperatures, it is necessary to investigate the changes in the droplet interface temperature as time progresses. In order to assess the temperature profile of the volatile pure and binary liquid sessile droplets at different substrate temperatures, IR thermography measurements were acquired. Experiments consist of depositing droplets of a known volume (from 1 to 5 ±0.2 μL) and initial temperature (9±1°C) on the uniformly heated glass substrate and recording the interface temperature map profile of the evaporating droplets. For IR data processing, a constant and homogeneous substrate temperature was assumed. Representative infrared temperature profile images of pure water and pure 1-butanol at substrate temperatures of ~30, ~60 and ~90 °C, are presented in Figures 8 and 9, respectively. They show the spatio-temporal evolution of temperature distribution along the interface of pure water and pure 1-butanol drops (with volumes of ~4±0.2 μL) at 0.05 s (upon initial deposition), 0.5 s and after 1 s, at constant temperature substrates. It is clear from the IR images that thermal energy is transferring from the contact line and propagates within the drop demonstrating that the top of the drop as the coldest point and the contact line the hottest region with the highest evaporation rate. In the case of the pure water droplets the thermal activity was found to be comparatively weaker than those of the pure 1-butanol droplets, as displayed in Figures 8 and 9. This was due to the different physical properties of the liquids. The generation of (Marangoni) convection cells (Figure 8) at the interface of the pure water droplets for 60°C substrate temperature, was observed at 1 s while for 90°C appeared clearly at 0.5 and 1 s. The appearance of these thermal patterns were attributed to the presence of thermal Marangoni convection where flows are driven from the contact line to the apex along the interface induced by tangential temperature gradients and then recirculated through the drop centre towards the contact line. This

24

phenomenon appeared to be clearer and more intensive when higher temperature gradients between the substrate (~90°C) and the liquid phase (~9°C) were applied. For the pure 1-butanol droplets the thermal patterns are centrosymmetric and ring-like closer to the contact line. As time evolved, after droplet deposition, the liquid surface temperature rapidly increased. The contact angle of the droplets decreased significantly after contact so does the liquid thickness, which relates to lower thermal resistance, and the evaporation rate of the system was remarkably increased. This led to faster depletion of the liquid phase. Therefore, at the vicinity of pure 1-butanol droplets' (approximate) contact line (dashed lines in Figure 9), the apparent emissivity became very small leading to higher uncertainty in the total energy that was emitted from the liquid phase due to energy reflected by both the liquid-vapour and the liquid-solid interfaces. Furthermore, as the 1-butanol is semi-transparent to infrared radiation at the wavelengths used from the camera (see also experimental section), the obtained IR measurements for the butanol cases reflected the temperature profile close at the liquid interface but not of the interface itself; thus the indicated temperatures must be interpreted with care.
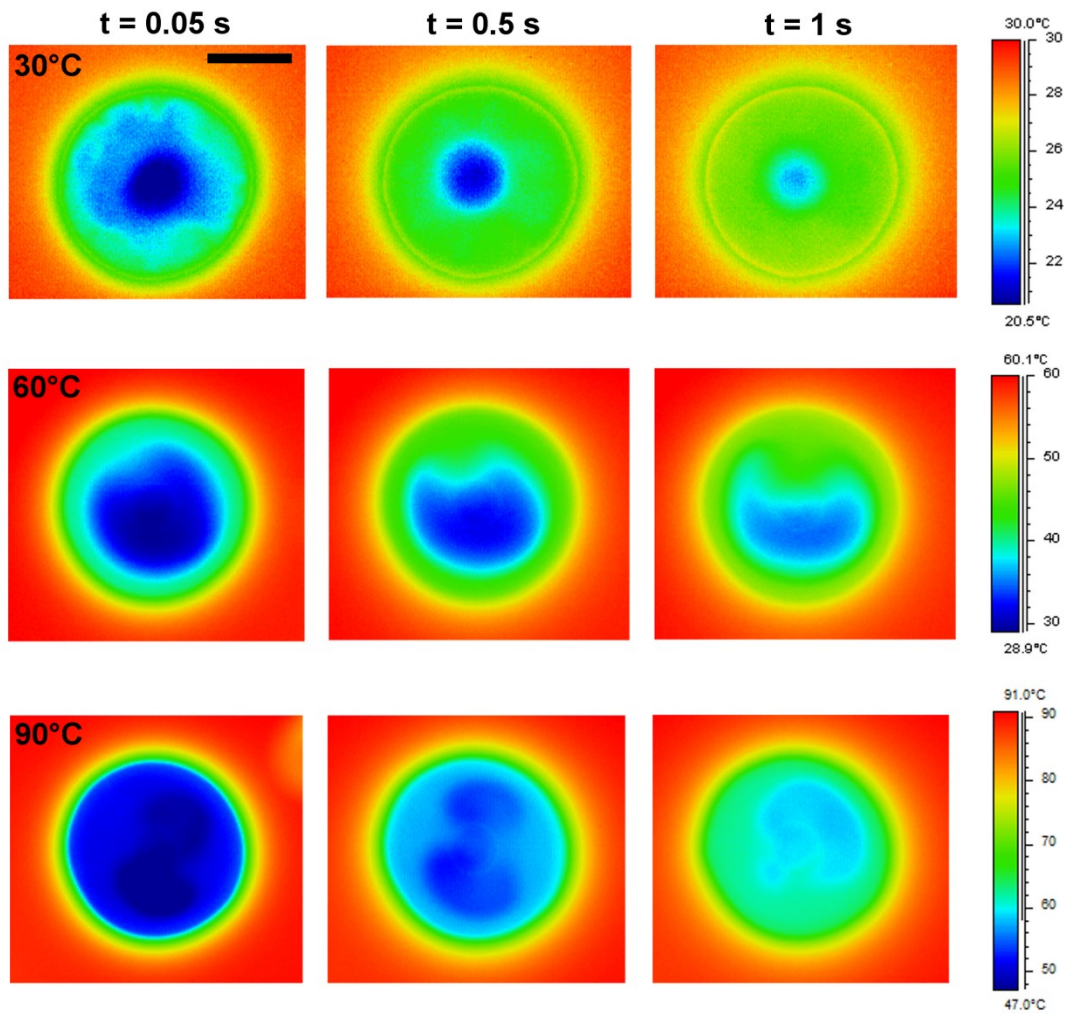
Figure 8. IR thermography visualizations of the temperature profile of sessile droplets (top view) of pure water (volumes of 4±0.2 μL) on a uniformly heated glass substrate at three different temperatures of ~30, ~60 and ~90 °C, immediately after deposition (0.05 s), after ~0.5 s and ~1 s. Note that the contrast in IR images at substrate temperature of around 30°C is not as sharp due to the lower temperature differences between the liquid droplets (interface) and the substrate. The scale bars depict a width of 1.5 mm, for each liquid case.
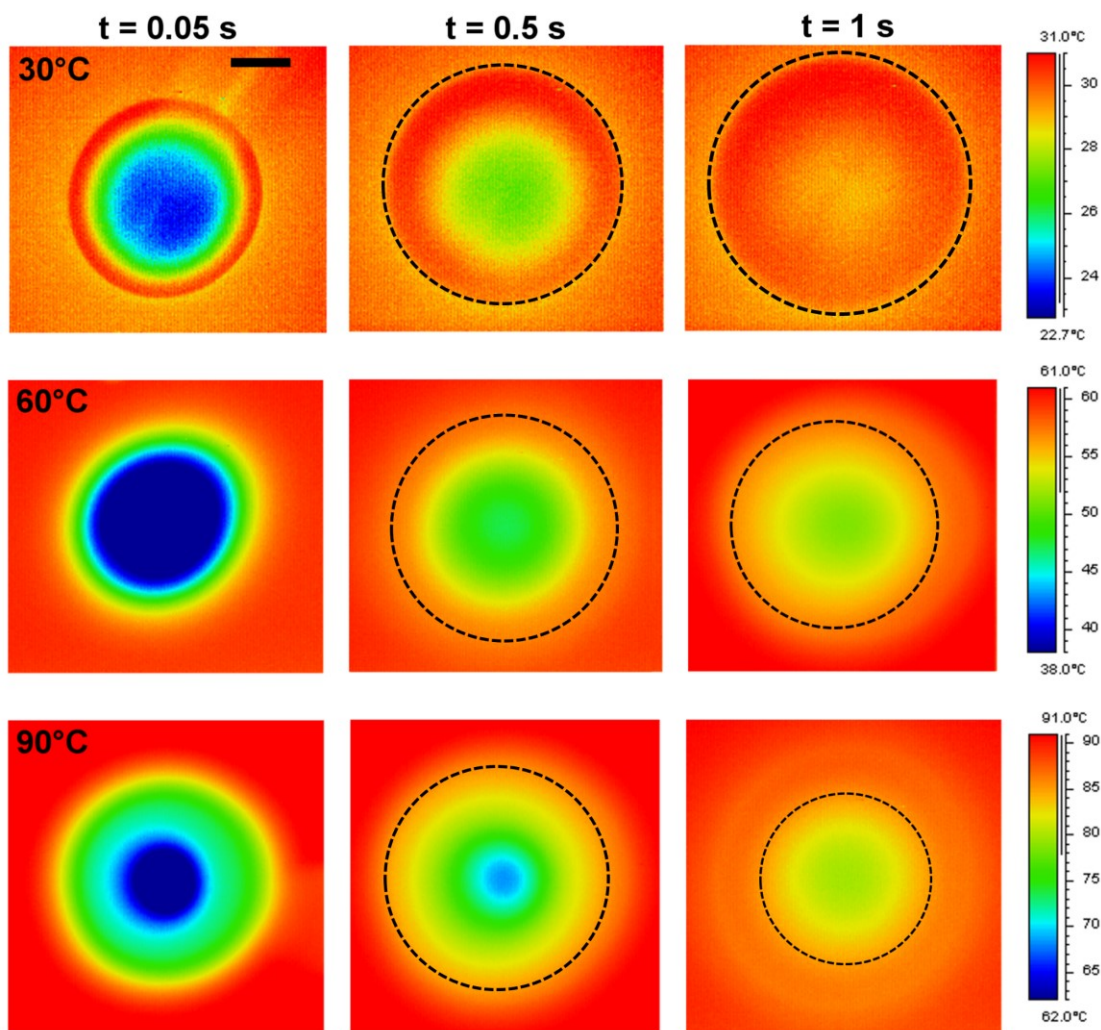
Figure 9. IR thermography visualizations of the temperature profile of sessile droplets (top view) of pure 1-butanol droplets (volumes of 4±0.2 μL) on a uniformly heated glass substrate at three different temperatures of ~30, ~60 and ~90 °C, immediately after deposition (0.05 s), after ~0.5 s and ~1 s. Note that the dashed lines represent the approximate moving contact line of the evaporating alcohol droplets. The scale bars depict a width of 1.5 mm, for each liquid case.

In Figure 10, we show the IR images for the water – 1-butanol 5% vol. droplets with volumes of around 4±0.2 μL at the three substrate temperatures: ~30, ~60 and ~90 °C. The generation of characteristic thermal patterns (heat convection from the edges toward to the centre) at the interface of the binary droplets can be clearly seen which

27

indicate that these droplets are in a transient phase with complex mixing, flows and boundary conditions between the two evaporating components (water and 1-butanol). The thermal patterns observed at a substrate temperatures of ~60°C and ~90°C are similar to each other, corresponding to a 'flowery' fluid-wave motion of alternating warm/cool regimes. The generated thermal patterns are characterized by relatively darker, curved bands (at the droplet edge), with a preferential direction of propagation towards the centre of the droplet owing to the presence of surface tension gradients. It is worthwhile noting that the development of these thermal patterns occurred spontaneously, upon the deposition of the binary droplets on the heated substrate and they were more pronounced at higher temperature differences between the droplet and the substrate. These observed thermal patterns are organised radially and circle around the apex of the evaporating-spreading droplet, in the region where most of evaporation occurs mainly of the alcohol component (more volatile). Moreover, Figures 11 and 12, depict further infrared visualization images for typical examples of the water – 1-butanol evaporating droplets at substrate temperatures of ~60°C and ~90°C, respectively, immediately after contact (~0.05 s), ~0.5 s (or 0.3 s), ~1 s and after ~3 s, where the generation of theses characteristic thermal instabilities within the evaporating self-rewetting droplets was further verified and more details of the process can be seen. Upon droplet deposition on the heated substrate, temperature gradients develop during the evaporation (and spreading) from the apex of the droplet and the contact line, resulting in surface tension gradients. Temperature (and/or composition) instabilities on the free fluid interface are known to generate Marangoni stresses and a flow that will drag the fluid from warm regions, where the surface tension is low, to cold regions, where the surface tension is high. The latter induces thermal-solutal convective phenomena within the droplet and these are observed as thermal patterns. In the initial

28

moments of the binary droplet spreading, the thermal field exhibited a very intricate and unbalanced evaporation-driven interfacial motion which covered completely the interface. As time progressed, this thermal motion gradually reduced its area of activity (decrease of temperature gradients) and finally disappeared completely following the characteristic motionless temperature field of pure water drops, as seen in Figure 8. The disappearance of these characteristic thermal patterns ($t > \sim 3$ s) can be determined as the moment of depletion of the alcohol phase (Figures 11 – 12). It is worthwhile noting that at later times of evaporation; ~ 3 s, at substrate temperatures of $\sim 60^{\circ}$C and $\sim 90^{\circ}$C, the presence of small random convection cells was observed which could be generated by the existence of thermal gradients (thermal Marangoni effect) within the droplets. Additionally, whatever is the stage of the evaporating droplets (both pure and binary liquids), the infrared visualization confirms the fact that the temperature of the droplet is hotter near the triple contact line and colder in the centre (apex).
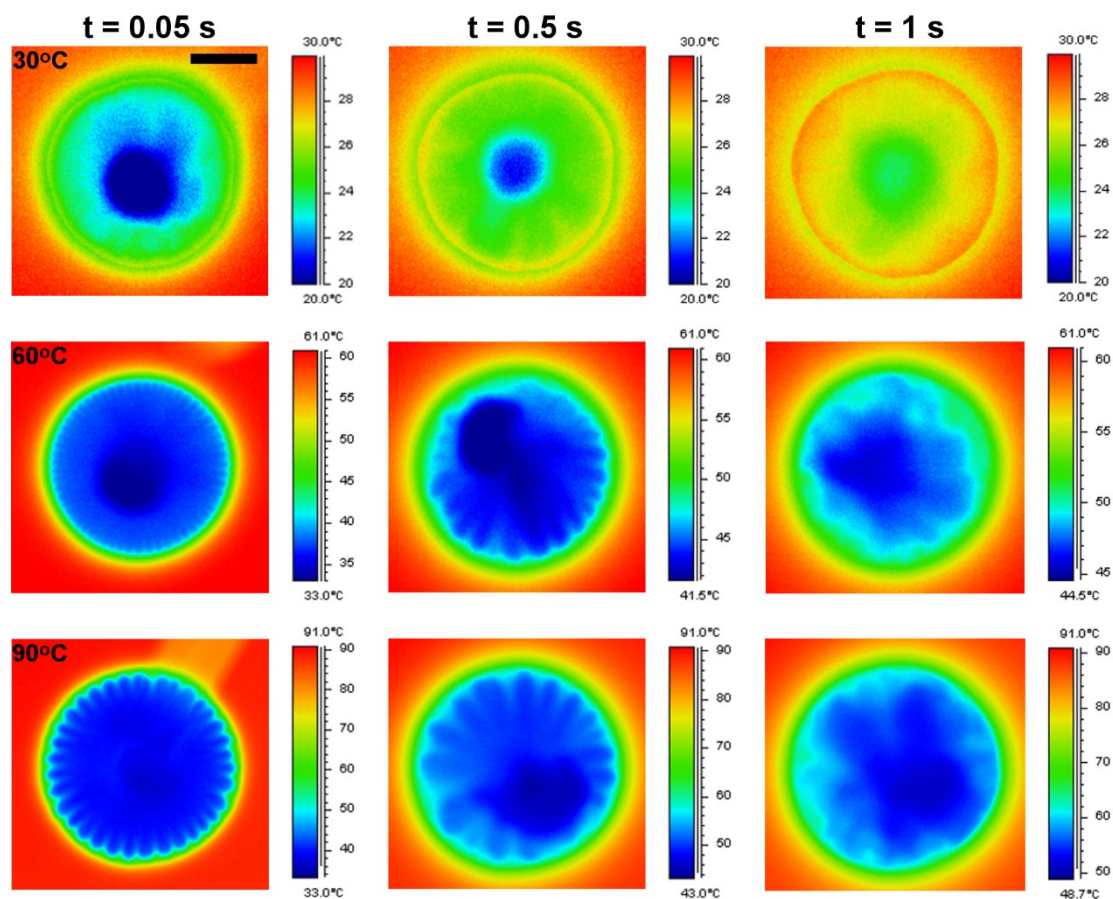
Figure 10. IR thermography visualizations of the temperature profile of sessile droplets (top view) of water - 1-butanol 5% vol. (volume of 4±0.2 μL) on a uniformly heated glass substrate at three different temperatures (~30, ~60 and ~90 °C) immediately after deposition, at ~0.5 s and after ~1 s. Note that the contrast in IR images at substrate temperature of ~30°C is not as sharp due to the lower temperature differences between the liquid droplets and the substrate. The scale bar depicts a width of 1 mm.
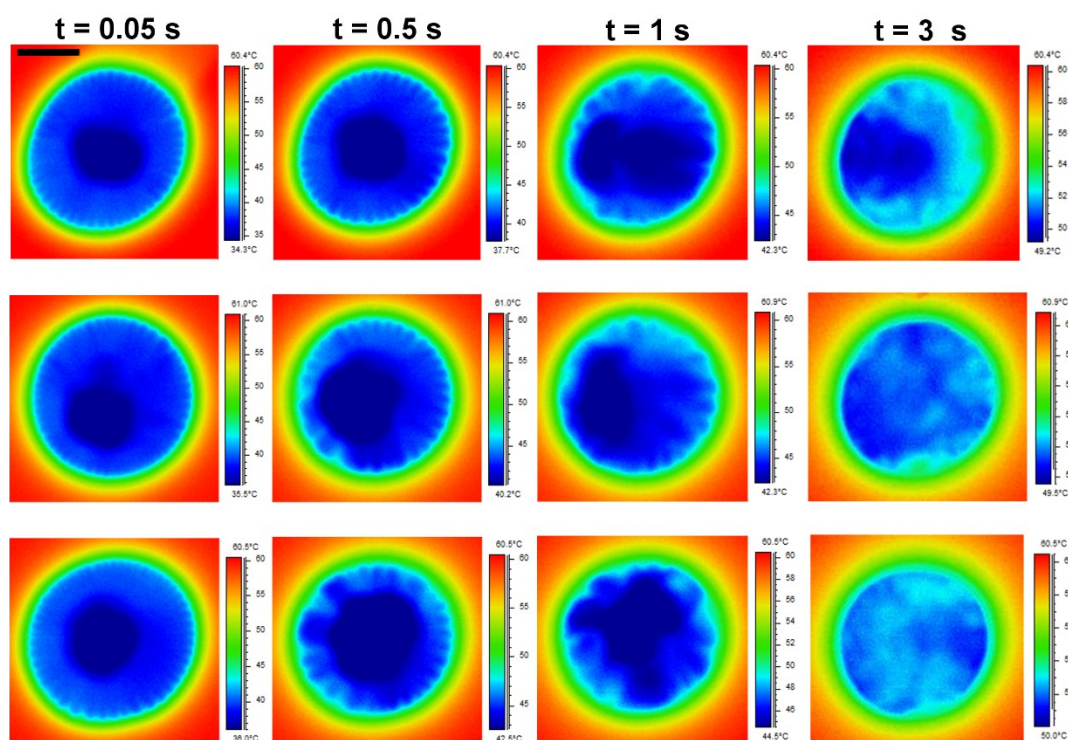
Figure 11. Infrared visualization images of the temperature profile of three sessile droplets (top view) of water – 1-butanol 5% vol. (volumes 4.5±0.2 μL) on a uniformly heated glass substrate at temperatures of ~60°C, immediately after contact (~0.05 s), ~0.5, ~1 and ~3 s. The scale bar depicts a width of 1.5 mm, for all images.
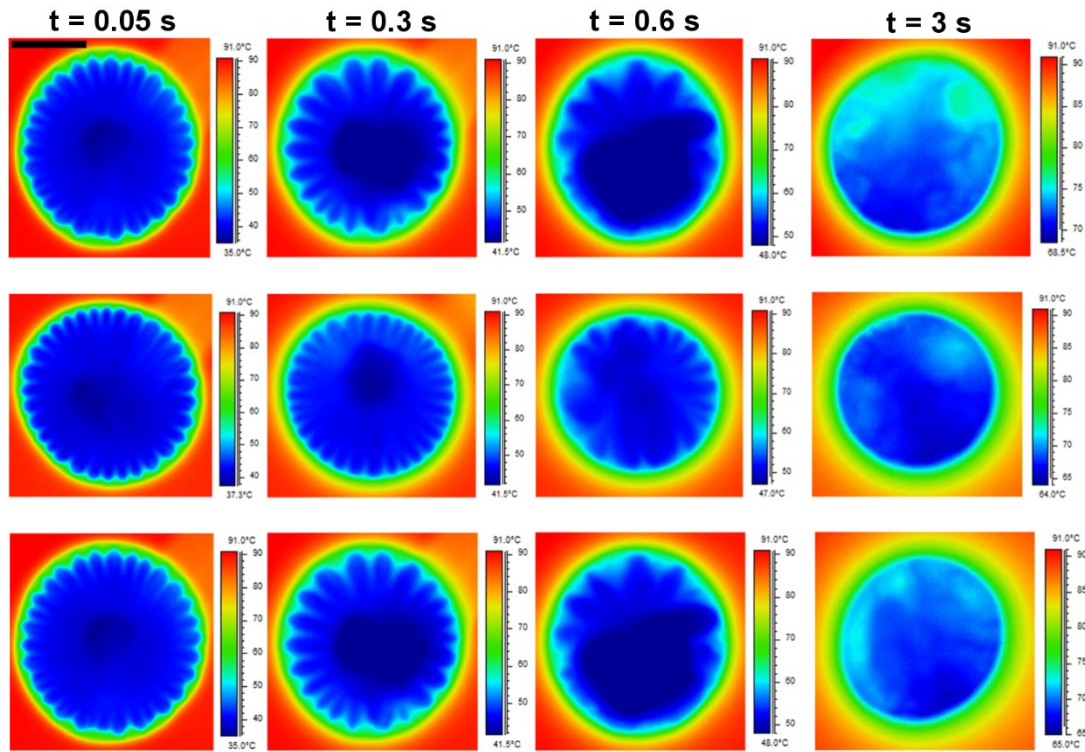
Figure 12. Infrared visualization images of the temperature profile of three sessile droplets (top view) of water – 1-butanol 5% vol. (volumes 4.6±0.2 μL) on a uniformly heated glass substrate at temperatures of ~90°C, immediately after contact (~0.05 s), ~0.3, ~0.6 and ~3 s. The scale bar depicts a width of 1.5 mm, for all images.

Additionally, the thermal activity of self-rewetting droplets; water-1-butanol 5% vol., on a different heated hydrophilic substrate was examined. Experiments consist of depositing spherical binary alcohol droplets on a heated ceramic (AlN) substrate (different thermal conductivity compared to glass substrate, ~100 times higher [65,66]) with volumes from around 3 to 5 ±0.2 μL and initial temperature 9±1°C, at two different substrate temperatures: ~60°C and ~90°C. The generation of characteristic thermal patterns (heat convection from the edges towards the centre) at the interface of the binary alcohol droplets, with volumes of 4±0.2 μL, at substrate temperatures of ~60°C and ~90°C, can be clearly observed in Figure 13 (a) and (b), respectively. The thermal patterns observed, on the ceramic substrate, at ~60°C and ~90°C, were similar to each

32

other, were described by a wave-fluid ('flowery') movement of characteristic warm/cool regions, which travelled inwards to the centre of the droplet; similar behaviour as seen in the case of glass substrate but clearly with more intensive formation and movement. The development of these thermal patterns occurred spontaneously, upon the deposition on the heated substrate and were more pronounced at higher temperature differences i.e. between the droplet and substrate. These gradients then generated thermocapillary instabilities within the binary droplet. The generated thermal patterns were portrayed by relatively darker flowery-bands, with a preferential direction of propagation waves towards the centre of the droplet and were organized radially around the apex, in the alcohol-rich region where most of the evaporation occurs. The wavelength of self-rewetting droplets was seen to increase when the substrate temperature was increased from 60°C to 90°C. The latter feature was observed for both substrates i.e. glass and ceramic, examined in this study. However, the wavelength of droplets depositing on the ceramic substrate compared to glass increased as the thermal conductivity of the ceramic is higher [65,66]. Furthermore, the binary droplets evaporating on the ceramic substrate reached a uniform temperature field much quicker (well before ~3 s) than those deposited on the glass surfaces owing to the higher heat transfer rate. The thermal activity and the generation-presence of characteristic thermal patterns i.e. number of waves, wavelength and intensity, at the interface of evaporating self-rewetting droplets was clearly affected from the substrate properties and the applied temperature.
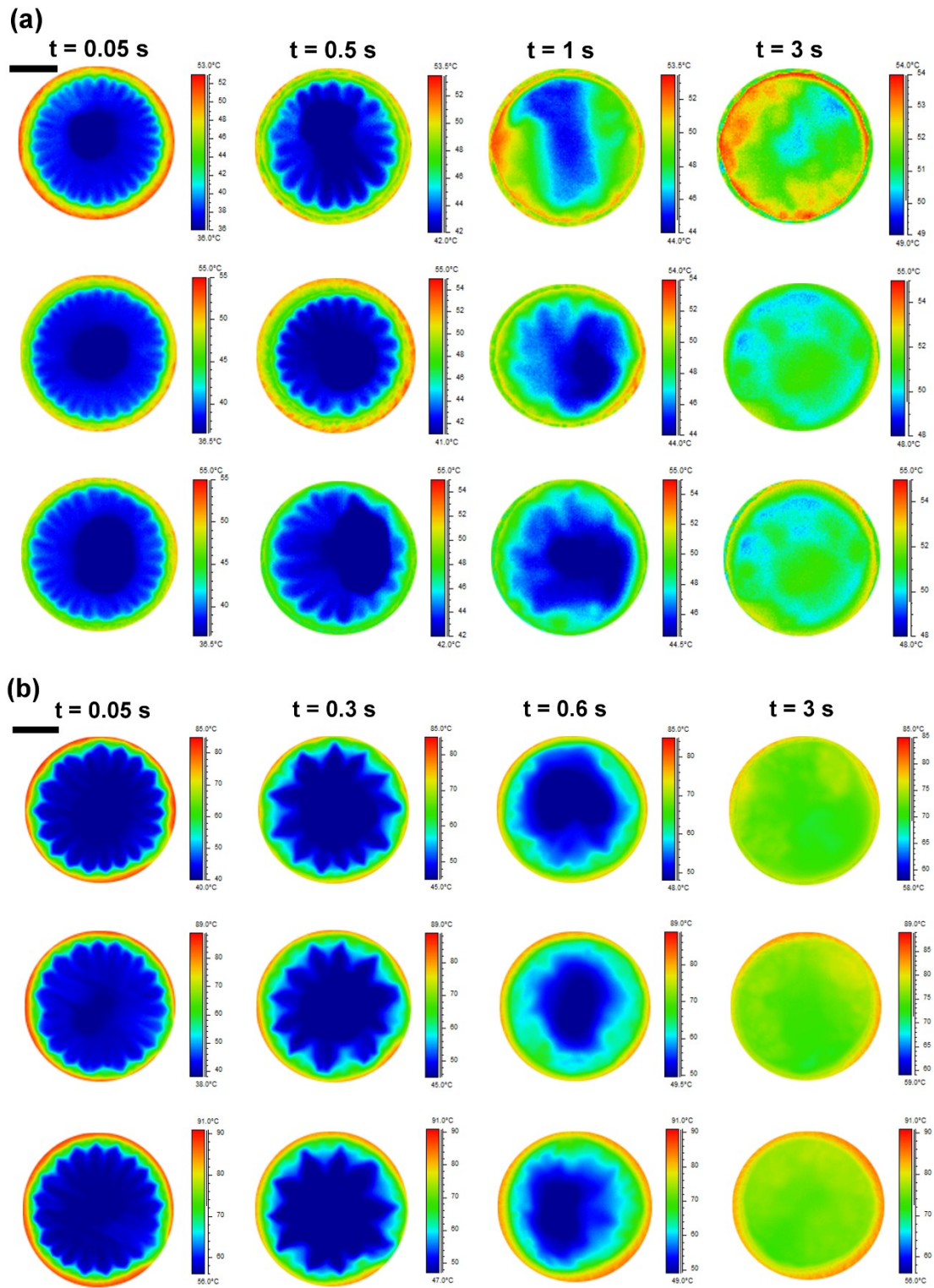
Figure 13. Infrared visualization images of the temperature profile of three sessile self-rewetting droplets i.e. water-1-butanol 5% vol., (top view) with volumes 4.5±0.2 μL, on a uniformly heated ceramic substrate at temperatures of (a) ~60°C and (b) ~90°C, immediately

after contact (~0.05 s) and 0.5 (at ~60ºC) or 0.3 (at ~90ºC), 1 and 3 s. The scale bar depicts a width of 1.5 mm, for all images.

The heat waves on the surface of the water-butanol droplets (with volumes from 4 to 4.5 ±0.2 µL, on glass and ceramic substrates) at two different temperatures: ~60ºC and ~90ºC, corresponding to the number of warmer (or cooler) curved-like regions, were visually counted and reported as a function of the dimensionless time t/t_{tot}, where t_{tot} is the duration of the thermal wave phenomena (time until the disappearance of the thermal waves), as shown in Figure 14 (a) and (b), respectively. Detailed inspection of these figures reveals that the number of waves depends drastically on the temperature of the substrate on which the binary droplets are deposited and also on the initial volume of the binary droplets. It is clear that the number of waves associated with the evaporation of the water-butanol droplet deposited on a ~60ºC substrate is larger than that of the droplet deposited on a ~90ºC substrate, both on glass and ceramic substrates. As the evaporative process proceeds, the number of waves formed follow an (approximately linear) decrease with time which is consistent with the driving mechanism of these thermal patterns. As the binary sessile droplet evaporated and heated up by the substrate, the overall concentration and temperature gradients along the free surface decreased which led to an accompanying decrease of the driving force of these patterns (Marangoni stresses). In the later stage of evaporation, the driving force (gradients) became sub-critical for the development of thermal patterns and it appeared difficult to follow those using the IR camera (Figures 10 – 13). The IR thermography visualizations of the temperature profile for water-1-pentanol sessile droplets on both substrates gave similar results to water-1-butanol droplets.
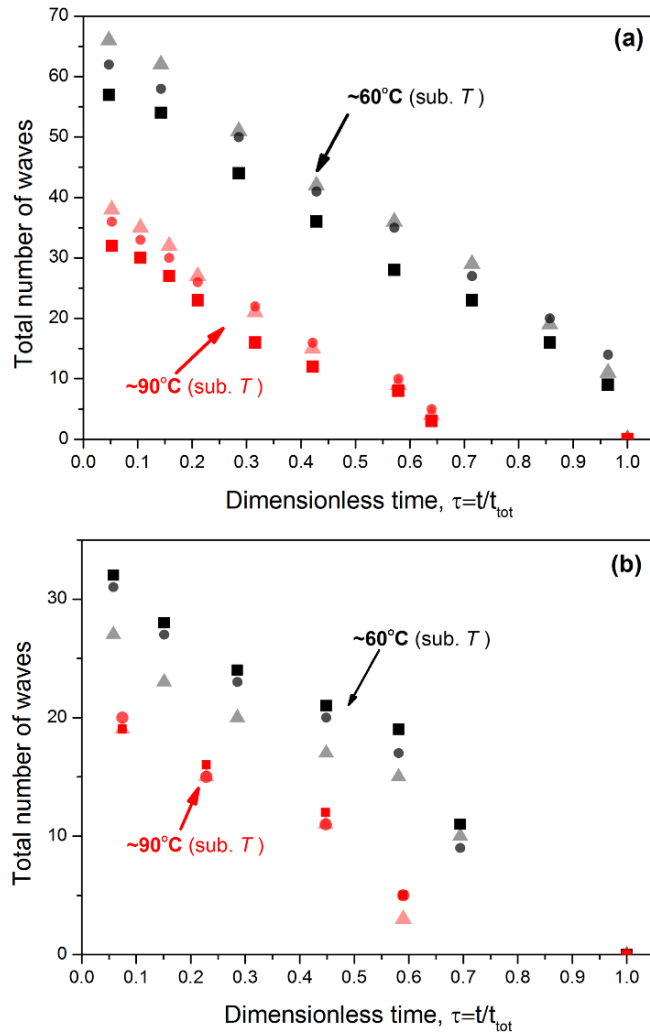
Figure 14. Temporal evolution of the number of observed thermal waves of six typical examples for water-1-butanol droplets (a) on glass substrate and (b) on ceramic substrate with volumes: 4 (■), 4.3 (●), 4.5 (▲) ±0.2 μL, and 4 (■), 4.3 (●) and 4.5 μL (▲) ±0.2 μL, at ~60°C and ~90°C substrate temperatures, respectively.

DISCUSSION

Generally, convection for volatile small drops, can be either gravity or surface tension driven (Marangoni effect). The capillary length is given by $l_c = \sqrt{\frac{\gamma}{\rho g}}$ (g is the acceleration of gravity and ρ liquid density) and therefore, for sessile droplets with

height $h < l_c$ (small droplets) Benard–Marangoni convection, surface tension forces at the liquid/air interface, was likely to dominate the effect of gravity. In the present study, we examined water-alcohol droplets with an initial height (as given by the height at the apex; largest droplet dimension) from ~0.5 to ~1.7 mm which is smaller than the capillary length, l_c calculated at around 1.9 mm. Thus, the convection mechanism at the early stages of spreading is unlikely to be buoyancy driven since the initial sizes of the droplets are small, i.e. below capillary length. This implies that the droplets will not be deformed by gravity and will adopt a spherical-cap shape. In turn, convection at the early stage of wetting is the result of surface-tension-driven flows either thremocapillary (temperature gradients) and/or solutal (concentration gradients) in nature and could not be described simply by evaporative flux, outward flow as suggested by Deegan *et al.* [9].

The spreading exponent of the early stage growth (n_{1st}) which determines the initial spreading speed rate was found to depend on the substrate temperature for all the liquids used. It is well-established that in evaporating sessile droplets, there is continuous outward flow driven by mass conservation [9] because of the higher evaporation rate near the triple contact line which leads to (small) temperature differences. In our experiments, at the early stages of wetting, the temperature differences between the triple-contact-line and the rest of the liquid phase were observed to be larger at higher temperatures as visually displayed in the IR thermography images (Figures 8 – 13). These temperature differences led to strong surface tension differences and thus to more intensive and agitated thermocapillary flows (Marangoni stresses) [10]. For pure liquids, the temperature dependence of the surface tension is linear (Figure 4 (a)) which leads to a linear increase of the spreading exponent when the temperature of the substrate is

increased (Figure 7 (a)). Interestingly, in the case of the alcohol mixtures, the non-monotonic dependence of the surface tension with the temperature (Figure 4 (b)) is associated with the exponent non-monotonic behaviour in the first (inertia-capillary) stage of spreading (Figure 7 (c)). The parabolic shape with a minimum at around 63°C of the surface tension – temperature curve (Figure 4 (b)) corresponds to a maximum wetting (Figure 3 (c) and (d)) of the evaporating self-rewetting droplets.

The evaporation of binary mixture droplets introduces a new additional effect in the system compared with the single-component droplets. As butanol (or pentanol) is more volatile than water and migrates to the liquid-air interface and leads to local concentration gradients along and across the interface of the droplet, resulting in surface tension stresses inducing additional solutal Marangoni flows which enhanced the generation of characteristic thermal waves as seen by IR thermography (Figures 10 – 13). In fact, any imposed temperature difference across the liquid-vapour interface of these binary mixtures created also local surface concentration gradients. These Marangoni instabilities induced flows away from regions with low surface tension in the direction of increasing surface tension (Figure 1) resulting in complex-agitated flows and thermal patterns. The patterns were more prominent for the higher temperature substrates leading to more clearly formed flowery-like bands as displayed in Figures 10 – 13.

It was only later, when the droplets approximately entered in Tanner's regime and the contact line dissipation was controlled by slow spreading dynamics where the exponents changed to lower values, as seen in Figure 7 (b) and (d). This stage of wetting (at a later phase of evaporation) was characterized by progressively fewer thermal

waves (until they disappeared) and the presence of slow contact line dynamics i.e. viscous-capillary regime, where the apparent exponent n reached a plateau with values $0.1 < n < 0.2$ in agreement with previous studies on other liquids for this wetting regime [39,40,42].

The characteristic thermal patterns observed in our experiments confirmed that the Marangoni instabilities induced characteristic thermal travelling waves and showed that the evaporation rate of these sessile water-alcohol droplets cannot be described by a vapour diffusion mechanism alone. The fact that the thermal patterns were more prominent for higher substrate temperatures indicates that the Marangoni-induced flows contributed more significantly to energy transport phenomena as the temperature differences were higher. By the end of the first stage (inertia-capillary region), most (if not all) of the alcohol phase (butanol or pentanol) would have evaporated and also the temperature differences over the droplet would have become smaller, as the capillary waves propagate within the droplet. Thus, concentration and temperature gradients appeared to be weak to sustain the flows and the solutal-thermacapillary Marangoni stresses became sub-critical. In addition, the frequency of observed thermal waves decreased as the droplets' heating and evaporation proceeded (Figure 14). Another feature revealed in this work was that the number of the thermal waves significantly decreased (but they were more intense) as the temperature of the substrate was increased as well as when the thermal conductivity of the substrate was higher.

Finally, it is worth noting that for short chain alcohol molecules (such as butanol and pentanol used in this study) the alcohol-rich phase has a tendency to completely wet the air-water interface; this tendency is more pronounced for shorter alcohol chain lengths

and at higher temperatures [67,68]. The shorter chain alcohol is characterised by a better surface activity at the interface separating air and the aqueous phase. Hence the transfer of alcohol molecules from the bulk phase to the interface is more energetically favourable for the shorter alcohol chain length. This may explain the different spreading exponents between the two binary mixtures (Figure 7 (c)) for higher substrate temperatures connected with the surface tension - temperature dependence and the generated surface tension gradients of these binary droplets.

CONCLUSIONS

We investigated the fluid contact line dynamics combined with infrared thermography imaging of evaporating sessile droplets of self-rewetting liquids under controlled experimental conditions. We have shown that the early stage of spreading on partially wetting substrates depends strongly on the substrate temperature. The exponent of the very first initial stage of spreading was close to 0.5 at substrate temperature of 30ºC and increased non-monotonically at higher temperatures. This is consistent with the anomalous surface tension behaviour (at a particular range of temperatures) of these self-rewetting liquids. The second stage exponents was found to be from around 0.1 to 0.2 consistent with the presence of a viscous-capillary balance regime. Furthermore, we observed the spontaneous appearance of characteristic thermal travelling waves which were developed along and across the free interface of the evaporating droplets. The latter was due to the spontaneous segregation of the more volatile components namely 1-butanol and 1-pentanol in the binary solutions. Surface-tension-driven (Marangoni convection) thermal patterns occurred and were attributed to the temperature and/or concentration gradients hence influencing significantly the early-times spreading dynamics. It was further verified that the applied temperature and the properties of the

substrate affected the orientation and intensity of the generated 'flowery' thermal patterns.

ASSOCIATED CONTENT

Supporting Information

ACKNOWLEDGMENTS

REFERENCES

(1)   de Gennes, P. G. Wetting: Statics and Dynamics. *Rev. Mod. Phys.* **1985**, *57* (3), 827–863.

(2)   Simpkins, P. G.; Kuck, V. J. On Air Entrainment in Coatings. *J. Colloid Interface Sci.* **2003**, *263* (2), 562–571.

(3)   de Gennes, P. G.; Brochard-Wyart, F.; Quéré, D. *Capillarity and Wetting Phenomena*, 1st ed.; Springer-Verlag New York, 2004.

(4)   Tabeling, P. Microfluidics/Microfluidique - Foreword. *Comptes Rendus Phys.* **2004**, *5* (5), 519–520.

(5)   Soltman, D.; Subramanian, V. Inkjet-Printed Line Morphologies and Temperature Control of the Coffee Ring Effect. *Langmuir* **2008**, *24* (5), 2224–2231.

(6)   Bonn, D.; Eggers, J.; Indekeu, J.; Meunier, J.; Rolley, E. Wetting and Spreading.

Rev. Mod. Phys. **2009**, *81*, 739.

(7)   Singh, M.; Haverinen, H. M.; Dhagat, P.; Jabbour, G. E. Inkjet Printing—
        Process and Its Applications. *Adv. Mater.* **2010**, *22* (6), 673–685.

(8)   Wijshoff, H. The Dynamics of the Piezo Inkjet Printhead Operation. *Phys. Rep.*
        2010, *491* (4–5), 77–177.

(9)   Deegan, R. D.; Bakajin, O.; Dupont, T. F.; Huber, G.; Nagel, S. R.; Witten, T.
        A. Capillary Flow as the Cause of Ring Stains from Dried Liquid Drops. *Nature*
        1997, *389* (6653), 827–829.

(10)   Hu, H.; Larson, R. G. Marangoni Effect Reverses Coffee-Ring Depositions. *J.
        Phys. Chem. B* **2006**, *110* (14), 7090–7094.

(11)   Sefiane, K.; Wilson, S. K.; David, S.; Dunn, G. J.; Duffy, B. R. On the Effect of
        the Atmosphere on the Evaporation of Sessile Droplets of Water. *Phys. Fluids*
        2009, *21* (6), 62101.

(12)   Erbil, H. Y. Evaporation of Pure Liquid Sessile and Spherical Suspended Drops:
        A Review. *Adv. Colloid Interface Sci.* **2012**, *170* (1–2), 67–86.

(13)   Fukatani, Y.; Orejon, D.; Kita, Y.; Takata, Y.; Kim, J.; Sefiane, K. Effect of
        Ambient Temperature and Relative Humidity on Interfacial Temperature during
        Early Stages of Drop Evaporation. *Phys. Rev. E* **2016**, *93* (4), 43103.

(14)   Brutin, D.; Sobac, B.; Rigollet, F.; Le Niliot, C. Infrared Visualization of
        Thermal Motion inside a Sessile Drop Deposited onto a Heated Surface. *Exp.
        Therm. Fluid Sci.* **2011**, *35* (3), 521–530.

(15)   Alizadeh, A.; Bahadur, V.; Zhong, S.; Shang, W.; Li, R.; Ruud, J.; Yamada, M.;
        Ge, L.; Dhinojwala, A.; Sohal, M. Temperature Dependent Droplet Impact
        Dynamics on Flat and Textured Surfaces. *Appl. Phys. Lett.* **2012**, *100* (11),
        111601.

(16)   Amini, A.; Homsy, G. M. Evaporation of Liquid Droplets on Solid Substrates. I.
        Flat Substrate with Pinned or Moving Contact Line. *Phys. Rev. Fluids* **2017**, *2*
        (4), 43603.

(17)   Deegan, R. D.; Bakajin, O.; Dupont, T. F.; Huber, G.; Nagel, S. R.; Witten, T.
        A. Contact Line Deposits in an Evaporating Drop. *Phys. Rev. E* **2000**, *62* (1),
        756–765.

(18)   Hamamoto, Y.; Christy, J. R.; Sefiane, K. Order-of-Magnitude Increase in Flow
        Velocity Driven by Mass Conservation during the Evaporation of Sessile Drops.
        Phys Rev E Stat Nonlin Soft Matter Phys **2011**, *83* (5), 51602.

(19) Bénard, H. Les Tourbillons Cellulaires Dans Une Nappe Liquide. - Méthodes Optiques D'observation et D'enregistrement. *J. Phys. Theor. Appl.* **1901**, *10* (1), 254–266.

(20) Pearson, J. R. A. On Convection Cells Induced by Surface Tension. *J. Fluid Mech.* **1958**, *4* (5), 489–500.

(21) Ghasemi, H.; Ward, C. A. Energy Transport by Thermocapillary Convection during Sessile-Water-Droplet Evaporation. *Phys. Rev. Lett.* **2010**, *105* (13), 136102.

(22) Ristenpart, W. D.; Kim, P. G.; Domingues, C.; Wan, J.; Stone, H. A. Influence of Substrate Conductivity on Circulation Reversal in Evaporating Drops. *Phys. Rev. Lett.* **2007**, *99* (23), 234502.

(23) Sáenz, P. J.; Sefiane, K.; Kim, J.; Matar, O. K.; Valluri, P. Evaporation of Sessile Drops: A Three-Dimensional Approach. *J. Fluid Mech.* **2015**, *772*, 705–739.

(24) Kita, Y.; Askounis, A.; Kohno, M.; Takata, Y.; Kim, J.; Sefiane, K. Induction of Marangoni Convection in Pure Water Drops. *Appl. Phys. Lett.* **2016**, *109* (17), 171602.

(25) Askounis, A.; Kita, Y.; Kohno, M.; Takata, Y.; Koutsos, V.; Sefiane, K. Influence of Local Heating on Marangoni Flows and Evaporation Kinetics of Pure Water Drops. *Langmuir* **2017**, *33* (23), 5666–5674.

(26) Sefiane, K.; David, S.; Shanahan, M. E. R. Wetting and Evaporation of Binary Mixture Drops. *J. Phys. Chem. B* **2008**, *112* (36), 11317–11323.

(27) Sefiane, K.; Tadrist, L.; Douglas, M. Experimental Study of Evaporating Water–ethanol Mixture Sessile Drop: Influence of Concentration. *Int. J. Heat Mass Transf.* **2003**, *46* (23), 4527–4534.

(28) Cheng, A. K. H.; Soolaman, D. M.; Yu, H. Z. Evaporation of Microdroplets of Ethanol−Water Mixtures on Gold Surfaces Modified with Self-Assembled Monolayers. *J. Phys. Chem. B* **2006**, *110* (23), 11267–11271.

(29) Shi, L.; Shen, P.; Zhang, D.; Lin, Q.; Jiang, Q. Wetting and Evaporation Behaviors of Water–ethanol Sessile Drops on PTFE Surfaces. *Surf. Interface Anal.* **2009**, *41* (12–13), 951–955.

(30) Liu, C.; Bonaccurso, E. Microcantilever Sensors for Monitoring the Evaporation of Microdrops of Pure Liquids and Mixtures. *Rev. Sci. Instrum.* **2010**, *81* (1), 13702.

(31) Rowan, S. M.; Newton, M. I.; Driewer, F. W.; McHale, G. Evaporation of

Microdroplets of Azeotropic Liquids. *J. Phys. Chem. B* **2000**, *104* (34), 8217–8220.

(32) Hamamoto, Y.; Christy, J. R. E.; Sefiane, K. The Flow Characteristics of an Evaporating Ethanol Water Mixture Droplet on a Glass Substrate. *J. Therm. Sci. Technol.* **2012**, *7* (3), 425–436.

(33) Bennacer, R.; Sefiane, K. Vortices, Dissipation and Flow Transition in Volatile Binary Drops. *J. Fluid Mech.* **2014**, *749*, 649–665.

(34) Schiaffino, S.; Sonin, A. A. Molten Droplet Deposition and Solidification at Low Weber Numbers. *Phys. Fluids* **1997**, *9* (11), 3172–3187.

(35) Soboleva, O. A.; Raud, E. A.; Summ, B. D. Initial-Stage of the Spreading of a Drop over a Solid-Surface . *Colloid J. Russ. Acad. Sci.* **1991**, *53* (6), 920–923.

(36) Soboleva, O. A.; Summ, B. D.; Raud, E. A. Transition from Inertial to Viscous Spreading of a Drop. *Colloid J. Ussr* **1989**, *51* (6), 1049–1052.

(37) Biance, A.-L.; Clanet, C.; Quéré, D. First Steps in the Spreading of a Liquid Droplet. *Phys. Rev. E* **2004**, *69* (1), 16301.

(38) Bird, J. C.; Mandre, S.; Stone, H. A. Short-Time Dynamics of Partial Wetting. *Phys. Rev. Lett.* **2008**, *100* (23), 234501.

(39) Rafaï, S.; Sarker, D.; Bergeron, V.; Meunier, J.; Bonn, D. Superspreading: Aqueous Surfactant Drops Spreading on Hydrophobic Surfaces. *Langmuir* **2002**, *18* (26), 10486–10488.

(40) Winkels, K. G.; Weijs, J. H.; Eddi, A.; Snoeijer, J. H. Initial Spreading of Low-Viscosity Drops on Partially Wetting Surfaces. *Phys. Rev. E* **2012**, *85* (5), 55301.

(41) Chen, L.; Auernhammer, G. K.; Bonaccurso, E. Short Time Wetting Dynamics on Soft Surfaces. *Soft Matter* **2011**, *7* (19), 9084.

(42) Courbin, L.; Bird, J. C.; Reyssat, M.; Stone, H. A. Dynamics of Wetting: From Inertial Spreading to Viscous Imbibition. *J. Phys. Condens. Matter* **2009**, *21* (46), 464127.

(43) Tanner, L. H. Spreading of Silicone Oil Drops on Horizontal Surfaces . *J. Phys. D-Applied Phys.* **1979**, *12* (9), 1473–1484.

(44) Vochten, R.; Petre, G. Study of the Heat of Reversible Adsorption at the Air-Solution Interface. II. Experimental Determination of the Heat of Reversible Adsorption of Some Alcohols. *J. Colloid Interface Sci.* **1973**, *42* (2), 320–327.

(45) Oron, A.; Rosenau, P. On a Nonlinear Thermocapillary Effect in Thin Liquid Layers. *J. Fluid Mech.* **1994**, *273*, 361–374.

(46) Slavtchev, S. G.; Miladinova, S. P. Thermocapillary Flow in a Liquid Layer at Minimum in Surface Tension. *Acta Mech.* **1998**, *127* (1–4), 209–224.

(47) Abe, Y.; Iwasaki, A.; Tanaka, K. Microgravity Experiments on Phase Change of Self-Rewetting Fluids. *Ann. N.Y. Acad. Sci.* **2004**, *1027*, 269.

(48) Abe, Y. Self-Rewetting Fluids. *Ann. N. Y. Acad. Sci.* **2006**, *1077* (1), 650–667.

(49) Cheng, K. K.; Park, C. Surface Tension of Dilute Alcohol-Aqueous Binary Fluids: N-Butanol/water, N-Pentanol/water, and N-Hexanol/water Solutions. *Heat Mass Transf.* **2017**, *53* (7), 2255–2263.

(50) Zhang, N. Innovative Heat Pipe Systems Using a New Working Fluid. *Int. Commun. Heat Mass Transf.* **2001**, *28* (8), 1025–1033.

(51) Savino, R.; Cecere, A.; Paola, R. D. Surface Tension Driven Flow in Wickless Heat Pipes with Self-Rewetting Fluids. *Int. J. Heat Fluid Flow* **2009**, *30*, 380.

(52) Savino, R.; Monti, R. Heat Pipes for Space Applications. *Sp. Technol.* **2005**, *25*, 59–61.

(53) Savino, R.; di Francescantonio, N.; Fortezza, R.; Abe, Y. Heat Pipes with Binary Mixtures and Inverse Marangoni Effects for Microgravity Applications. *Acta Astronaut.* **2007**, *61* (1–6), 16–26.

(54) Savino, R.; Paterna, D. Marangoni Effect and Heat Pipe Dry-Out. *Phys. Fluids* **2006**, *18* (11), 118103.

(55) di Francescantonio, N.; Savino, R.; Abe, Y. New Alcohol Solutions for Heat Pipes: Marangoni Effect and Heat Transfer Enhancement. *Int. J. Heat Mass Transf.* **2008**, *51* (25–26), 6199–6207.

(56) Tanaka, K.; Abe, Y.; Nakagawa, M.; Piccolo, C.; Savino, R. Low-Gravity Experiments of Lightweight Flexible Heat Pipe Panels with Self-Rewetting Fluids. *Ann. N. Y. Acad. Sci.* **2009**, *1161* (1), 554–561.

(57) Di Paola, R.; Savino, R.; Mirabile Gattia, D.; Marazzi, R.; Vittori Antisari, M. Self-Rewetting Carbon Nanofluid as Working Fluid for Space and Terrestrial Heat Pipes. *J. Nanoparticle Res.* **2011**, *13* (11), 6207–6216.

(58) Hu, Y.; Liu, T.; Li, X.; Wang, S. Heat Transfer Enhancement of Micro Oscillating Heat Pipes with Self-Rewetting Fluid. *Int. J. Heat Mass Transf.* **2014**, *70*, 496–503.

(59) Ouenzerfi, S.; Harmand, S. Experimental Droplet Study of Inverted Marangoni Effect of a Binary Liquid Mixture on a Nonuniform Heated Substrate. *Langmuir* **2016**, *32* (10), 2378–2388.

(60) Chen, P.; Harmand, S.; Ouenzerfi, S.; Schiffler, J. Marangoni Flow Induced Evaporation Enhancement on Binary Sessile Drops. *J. Phys. Chem. B* **2017**, *121* (23), 5824–5834.

(61) Mamalis, D.; Koutsos, V.; Sefiane, K. On the Motion of a Sessile Drop on an Incline: Effect of Non-Monotonic Thermocapillary Stresses. *Appl. Phys. Lett.* **2016**, *109* (23), 231601.

(62) Mamalis, D.; Koutsos, V.; Sefiane, K. Bubble Rise in a Non-Isothermal Self-Rewetting Fluid and the Role of Thermocapillarity. *Int. J. Therm. Sci.* **2017**, *117*, 146–162.

(63) Rotenberg, Y.; Boruvka, L.; Neumann, A. W. Determination of Surface Tension and Contact Angle from the Shapes of Axisymmetric Fluid Interfaces. *J. Colloid Interface Sci.* **1983**, *93* (1), 169–183.

(64) Hu, H.; Larson, R. G. Analysis of the Microfluid Flow in an Evaporating Sessile Droplet. **2005**.

(65) Jarrige, J.; Lecompte, J. P.; Mullot, J.; Müller, G. Effect of Oxygen on the Thermal Conductivity of Aluminium Nitride Ceramics. *J. Eur. Ceram. Soc.* **1997**, *17* (15), 1891–1895.

(66) Jarrige, J.; Mexmain, J.; Oumaloul, M.; Bachelard, R.; Disson, J. P. Le Nitrure D'aluminium : De La Poudre Au Substrat. *J. Phys. III Fr.* **1993**, *3* (4), 703–712.

(67) Yeh, M.-C.; Lin, P.-C.; Chen, L.-J. Effect of Molecular Structure on Wetting Behavior at the Air−Liquid Interface of Water + Alcohol Mixtures. *J. Phys. Chem. B* **2004**, *108* (28), 9955–9961.

(68) Aratono, M.; Takayuki, T.; Takeo, S.; Ikeda, N.; Takiue, T. Dihedral Angle of Lens and Interfacial Tension of Air/Long Chain Alcohol/Water Systems. **1997**.